Additive manufacturing of thermoelectric materials via fused filament fabrication

Cagri Oztan [a], Sedat Ballikaya [b], Umit Ozgun [b], Ryan Karkkainen [a], Emrah Celik [a,*]

[a] Department of Mechanical and Aerospace Engineering, University of Miami, USA
[b] Department of Electrical and Electronics Engineering, Istanbul University, Turkey

ARTICLE INFO

ABSTRACT

Fused filament fabrication (FFF) is a commonly adopted additive manufacturing technique which allows direct assembly of intricate 3D multi-material components at high resolution and low cost. The aim of this research is to explore FFF processes and their unique capabilities in development of highly efficient thermoelectric (TE) energy harvesting material systems. Adapted fused filament fabrication with customized filaments produced samples with ABS (acrylonitrile butadiene styrene) polymer matrix and Bi_2Te_3 as the thermoelectric agent. Mixtures were initially extruded into composite thermoelectric filaments, which were subsequently printed into shapes and sintered in a tube furnace under inert gas environment. Thermoelectric performance characterization of the samples revealed that a maximum figure of merit of 0.54 was achieved at the sintering temperature of 500 °C for room temperature operation. This conversion efficiency was nearly five times higher than those of previously reported additively manufactured thermoelectric materials. The FFF method was therefore proven as a versatile method to fabricate efficient thermoelectric materials in intricate geometries.

1. Introduction

Over 68% of the energy produced in the United States is eventually rejected to the environment and ultimately goes unused in terms of waste heat [1]. A promising method of reclaiming energy waste is to use thermoelectric (TE) energy harvesters, which are multi-material solid-state devices that convert heat (i.e. a thermal gradient) directly into electric potential. Thermoelectric devices are in use today as Peltier coolers, body-heat energy harvesters, automotive applications, high-power industrial heat harvesters, solar-thermal systems for space travel, and thermal sensors [2,3]. These systems utilize the Seebeck effect, where a temperature gradient across the material causes charge carriers to move from the hot side to the cold side, thereby creating an electrostatic potential [4]. The dimensionless thermoelectric figure of merit, *ZT*, is used to characterize the effectiveness of a thermoelectric material with the following relationship:

$$ZT = \frac{S^2\sigma}{\kappa}T \tag{1}$$

where *S* is Seebeck coefficient, which denotes the capability of the material to convert temperature gradient into electric potential, *T* is absolute temperature, σ is electrical conductivity, and κ is the total thermal conductivity ($\kappa = \kappa_e + \kappa_L$ where κ_e is the electronic contribution and κ_L the lattice contribution). According to (1), high efficiency of a thermoelectric material requires high power factor ($S^2\sigma$) and low thermal conductivity at a specific operation temperature. Bismuth telluride (Bi_2Te_3) is one of the commonly used thermoelectric materials [5–7] for room-temperature applications and has been widely studied due to its *ZT* values around one [8].

The conventional manufacturing of thermoelectric devices is a laborious multistep process, which involves powder synthesis, leg dicing, and serial connection of numerous *p* and *n* type thermoelectric legs; this requires use of sophisticated equipment. This manufacturing technique has several drawbacks: it is limited only to planar, rectangular geometries [9], it is time consuming for large-scale integration, and it results in material loss during the process [4,10]. As a remedy to reduce the hassle of thermoelectric manufacturing and obtain complex thermoelectric device geometries, 3D printing technologies offer major advantages [11] such as fabrication without retooling, increased design freedom with complex geometries and flexible process parameters. Thermoelectric materials can be deposited in a layer-by-layer fashion by computer-controlled algorithm with minimal waste as well as easy alteration of scale and geometry. Recently, additive manufacturing techniques have been used to fabricate thermoelectric materials in

* Corresponding Author. Address: 1251 Memorial Drive, Coral Fables, FL, 33146, USA.
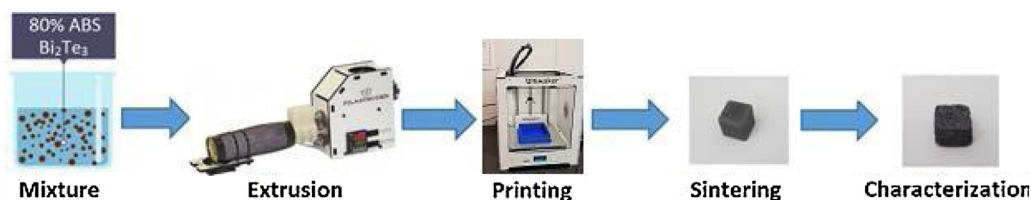*E-mail address:* e.celik@miami.edu (E. Celik).

Fig. 1. Schematic representation of fabrication of sintered samples.

terms of thin films and thick components. Solution-based processes such as ink printing [12–15] and screen printing [16–20] have been demonstrated as effective methods easily altering scale and geometry. These techniques, however, have low power capabilities, high electrical interconnect resistance, and weak mechanical properties due to high porosity.

Printing thicker components can alleviate these issues. Screen printing and extrusion based dispenser printing were employed to fabricate thermoelectric energy generators using Bi_2Te_3 [21,22]. Similarly, He et al. demonstrated the fabrication of thermoelectric bismuth antimony telluride ($Bi_{0.5}Sb_{1.5}Te_3$ or BST) samples by stereolithography, where a photoresin containing a dispersion of solid BST nanoparticles in loading ratios up to 60% can be printed in a 3D shape and then thermally annealed to leave behind only BST [23]. Dispenser printing and stereolithography are promising methods to additively manufacture thick thermoelectric components. However, they both suffer from poor thermoelectric performance compared to conventional fabrication methods, having an order of magnitude lower figure of merit (ZT) values.

In addition to these, selective laser sintering (SLA) and melting (SLM) are two emerging technologies recently employed to fabricate thermoelectric samples with complex geometries [24]. These techniques are based on deposition of a thin layer of powder followed by melting using a laser beam and subsequent solidification [25]. This method has also been utilized in various research studies [26–29]. Despite allowing fabrication of thermoelectric materials with complex geometries, such techniques require high initial investment costs for the equipment [30].

In this study, we investigate an alternative 3D printing methodology, fused filament fabrication (FFF), for cost-effective and versatile manufacturing of thermoelectric materials. FFF is a commonly used and well-established, commercialized method of manufacturing 3D polymer parts by melting a solid thermoplastic filament and depositing successive layers that fuse to a continuous profile [31]. The main advantages of FFF are its low cost, high resolution, and wide range of applicable materials. Previously, Wang et al. fabricated polylactic acid (PLA) based thermoelectric filaments using $Bi_{0.5}Sb_{1.5}Te_3$ with silane coupling agent, plasticizer, and multi-walled carbon nanotubes to ensure decent thermoelectric and mechanical properties for printing, but the filament was not utilized for printing [32].

This research focuses on FFF printing of a commonly used thermoelectric material (Bi_2Te_3) which was mixed with a sacrificial thermoplastic printing aide acrylonitrile butadiene styrene (ABS) powder for extrusion into thermoelectric filament that was subsequently printed, sintered, and characterized for thermoelectric and mechanical properties. Additionally, comparison with the previous studies was reported.

2. Material and methods

2.1. Filament fabrication and 3D printing

We followed a multistep experimental procedure for the fused filament fabrication of thermoelectric materials as described in

Fig. 1. It involved fabrication of thermoelectric composite filament (pre-process), 3D printing and sintering (post-processing). Bismuthtelluride powder with a size of 325 mesh (<44 μm) was purchased from Santech Materials, Hunan, China. Supplementary Fig. 1 shows the size and morphology of the powder. ABS polymer pellets were purchased from Filastruder Inc., GA, USA and cryogenically ground into powder (400 μm average size) to ensure as uniform blending as possible. In the initial step of the sample fabrication, Bi_2Te_3 powder was mixed with ABS powder and then fed into the hopper of an extruder (Filastruder) which was set to an extrusion temperature of 220 °C. The resultant custom filament was then used as stock for the Ultimaker 2 printer. Infill ratio, layer height and printing speed were set to 100%, 0.2 mm and 40 mm/s, respectively. The mass fraction of Bi_2Te_3 to ABS in all mixtures was maintained at 80 percent for higher ratios resulted with excessively brittle filaments that fractured in the tube of the 3D printer. The temperature of the nozzle with a diameter of 0.4 mm was maintained at 260 °C. The heat bed on which the material is deposited was set to a temperature of 90 °C. Double-sided tape was applied to ensure first-layer adhesion. Cubes with an edge of 10 mm were printed.

2.2. Heat treatment and sintering

Printed specimens were subsequently sintered in an MTI OTF-1200X tube furnace, to accomplish two main objectives: (1) removal of the polymer matrix from the prints, (2) fusing of the remaining Bi_2Te_3 particles together, which would lead to an improvement in the electrical conductivity due to enhanced contact between particles. Printed but unsintered specimens have very low electrical conductivity values, almost 3 orders of magnitude lower than the sintered specimens (Supplementary Fig. 2). In order to prevent oxidation of Bi_2Te_3, which exhibits high affinity to this, sintering was performed under high purity and ultra-high purity Argon environments. Initial sintering experiments in high purity argon (99.9% purity) atmosphere inside the tube furnace caused visible oxidation on the samples; as such, actual experiments were performed under ultra-high purity argon (99.9999% purity). In order to achieve additional reduction in oxidation, printed specimens were placed in brass enclosures, which acted as sacrificial protectors against oxidation due to higher tendency of oxidation. Using ultra-high purity argon and brass enclosure significantly mitigated the oxidation problem in the sintering process. The heating rate and the sintering duration of the furnace were set to 7 °C/h and 2 h, respectively (Supplementary Fig. 3). In order to investigate the effect of temperature on thermoelectric properties, 4 different sintering temperatures were selected; 450 °C, 500 °C, 550 °C and 575 °C. Maximum temperature of 575 °C was used considering that the melting point of Bi_2Te_3 is 585 °C [33]. Sintering temperatures below 450 °C were insufficient for the polymer matrix to be removed.

2.3. Thermoelectric and mechanical characterization

Commercial thermoelectric materials necessitate appreciable compressive strength levels since they are exposed to compressive

stresses between ceramic insulators. Thus, as-printed and sintered samples were tested to determine their out-of-plane compressive strength in accordance with ASTM C1424 standard. Out of plane direction was selected as the test direction since the mechanical properties are weakest at out of plane (z) printing direction. Printing filament flexural properties are also important to assess its usability within the tube of the printer, which requires adequate flexibility. Therefore, extruded filaments were characterized in terms of flexural properties via ASTM D790 tests where the flexibility, stiffness and strength properties were characterized.

Seebeck coefficient and electrical conductivity of the specimens were measured using Ulvac ZEM 3-M8 commercial equipment, which is capable of attaining a maximum temperature of 800 °C. The measurements were carried out in absence of deposited metal contact layers on the samples on which helium gas was purged. The total thermal conductivity (k) of each specimen was calculated using the following relationship:

$$k = D \cdot C_p \cdot p \qquad (2)$$

where D is the thermal diffusivity, Cp is the specific heat capacity and ρ is density of mass. Thermal diffusivity was measured using a commercial laser flash thermal diffusivity equipment (LFA 1100 Linseis). Specific heat was measured by a differential scanning calorimeter (Linseis-PT1000), and density was obtained from the Archimedes' method.

2.4. Imaging of microstructure and elemental analysis

A Jeol JSM-5600 LV model scanning electron microscope (SEM) was used to characterize morphology of the sintered Bi2Te3 specimens to make correlations with fabrication processes and ultimate performance. Sintered specimens were mechanically loaded until fracture, after which the cross-sections where failure occurred were imaged in the microscope. Finally, energy-dispersive X-ray spectroscopy (EDX) analysis was performed to detect the presence of oxidation and retaining polymer particles, along with the thermoelectric elements (Bi, Te) inside the microstructure.

3. Results and discussion

3.1. Mechanical testing

Supplementary Fig. 4 depicts the results of the compression test in which the as-printed samples reached a peak strength of 46.53 MPa. Highest strength among the sintered specimens was 33.14 MPa marked by the sintering temperature of 500 °C, which was 40% lower than the as-printed samples. All sintered samples exhibited compressive strains between a range of 0.3 and 0.4 mm/mm.

Supplementary Table 1 and Supplementary Fig. 5 summarize the flexural strength of the filaments and comparison thereof to Wang et al. [32]. Despite the absence of a reinforcement such as the ones used by Wang et al., extruded filaments manifested adequate flexural properties for use as a stock material in the tube of the printer.

3.2. SEM analysis of microstructure and composition

SEM pictures of the sintered specimens are shown in Fig. 2. According to these images, ABS matrix was successfully removed out of the specimens except for the sintering temperature of 450 °C, where retained ABS particles are clearly visible in Fig. 2A (labeled with white arrows). Additionally, sintering temperature significantly affected the microstructure of the printed samples. As the sintering temperature increased (500–550 °C), higher order of porosity was observed in the samples due to the removal of ABS particles. As a result, density of the samples reduced nearly 5% as shown in Supplementary Fig. 6. At the highest sintering
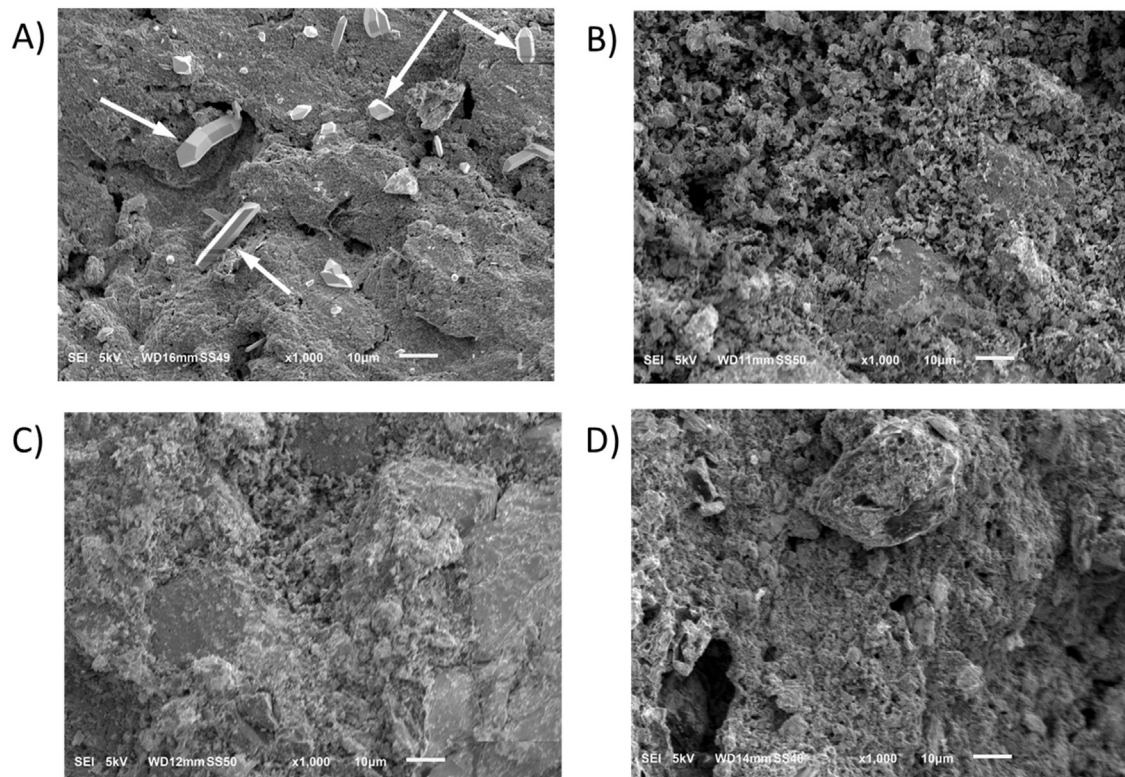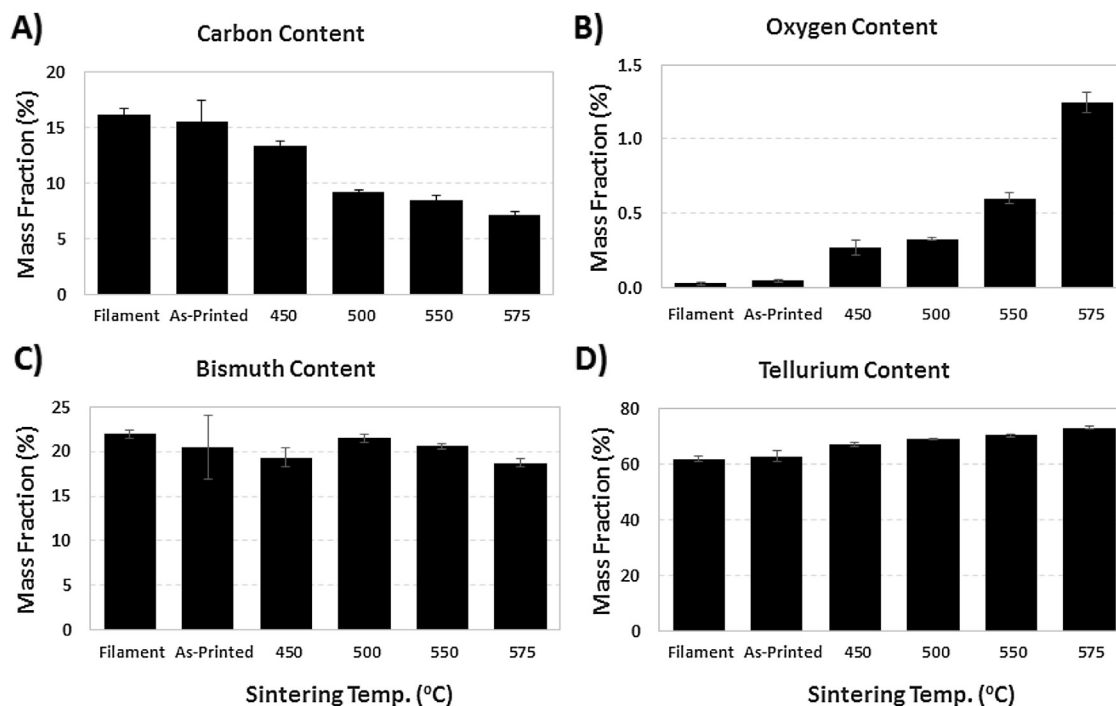

Fig. 2. SEM micrographs of sintered thermoelectric samples sintered at (A) 450 °C (retaining ABS particles are shown with the arrows), (B) 500 °C; (C) 550 °C, and (D) 575 °C.

Fig. 3. SEM-EDX Elemental analysis results as a function of sintering temperature: (A) carbon mass fraction, (B) oxygen mass fraction, (C) bismuth mass fraction, and (D) tellurium mass fraction.

temperature (575 °C) porosity was dramatically increased and larger voids were visible in Fig. 2D. Density also sharply decreased nearly to 16% of the samples sintered at 450 °C. Reduced density at this temperature could be due to disintegration of the Bismuth Telluride at temperatures close to the melting point of 585 °C and/or further removal of the polymer particles at this temperature.

EDX elemental X-ray analysis results in Fig. 3 showed two distinct changes in the samples at various sintering temperatures. As per Fig. 3A, oxidation level, which was approximately 0.1% by mass upon printing under 260 °C, dramatically increased with the increasing sintering temperatures reaching a peak of six times the amount obtained for the lowest sintering temperature of 450 °C. Oxidation in extruded filaments remained more than 90% below those of sintered. In addition to this, the mass fraction of the carbon element was significantly higher for the samples that were not sintered. As for sintered samples, it was highest in the minimum temperature (450 °C) and reduced significantly at higher temperatures. This result further proved the image analysis described in Fig. 2A that there were retained ABS particles in the samples sintered at 450 °C and higher sintering temperatures are necessary for the polymer burnout process. The main elements of the bismuth and tellurium remained nearly constant for all specimens in these tests. Change of oxygen mass fraction due to oxidation process and carbon content due to polymer burnout significantly affected the thermoelectric properties, which will be discussed in the subsequent section.

3.3. Thermoelectric characterization of sintered samples

Thermoelectric properties of the 3D printed specimens are given in Fig. 4 as a function of testing temperatures. Fig. 4A indicates the variation of Seebeck coefficient as a function of temperature in each sintering condition. The highest Seebeck coefficient was marked by the specimens sintered at 450 °C at room temperature. Seebeck coefficient of the specimens sintered at 500 °C remained below the former for operation temperatures less than 100 °C. Specimens sintered at 450 °C demonstrated continuously decreasing behavior

over temperature with the highest Seebeck coefficient of 265 μV/K at room temperature. Conversely, the specimens that were sintered at 500 °C, 550 °C and 575 °C exhibited parabolic behavior that reached peak values at 100 °C, 230 °C and 160 °C, respectively. Seebeck coefficients of 3D printed specimens sintered at 450 °C and 500 °C were in comparable range to that of bulk Bismuth Telluride.

Fig. 4B demonstrates the trend of electrical conductivity coefficient with respect to temperature for each sintering temperature. According to this figure, specimens sintered at 450 °C showed the minimum conductivity. Specimens sintered at 500 °C initially achieved the highest electrical conductivity of 54.66 S/cm, which was later surpassed by the specimens sintered at 550 °C until the operation temperature of 250 °C, where both were almost equally conductive with values of 29.44 S/cm and 28.67 S/cm. Specimens sintered at 575 °C displayed a mediocre electrical conductivity behavior of continuous decrease from 29.29 S/cm to 14.21 S/cm. Electrical conductivity of the printed specimens was found to be significantly lower than that of bulk bismuth telluride (1100 S/cm). This is due to the lower density and higher porosity level of the printed samples compared to bismuth telluride samples fabricated via conventional methods. As expected, electrical conductivity decreased with the higher sintering temperature since the porosity increased in these specimens as shown SEM images and density measurements (Fig. 2 and Supplementary Fig. 6). Reduction in electrical conductivity at high temperature can also be explained by the 3 to 5 fold increase in oxidation at higher temperatures as shown in Fig. 3. Detrimental effects of oxidation on electrical conductivity of thermoelectric materials at sintering temperatures over 500 °C were also observed in previous research studies [34–37].

Variation of thermal conductivity for the printed samples is given in Fig. 4C. According to this figure, thermal conductivities of the specimens were minimum at room temperature. Specimens sintered at 450 °C and 550 °C exhibited the lowest thermal conductivity. Nevertheless, thermal conductivity of all the printed specimens were found to be significantly lower than the bulk bismuth telluride thermal conductivity (1.1 W/mK) because of the porous structure of the printed specimens. Increasing thermal
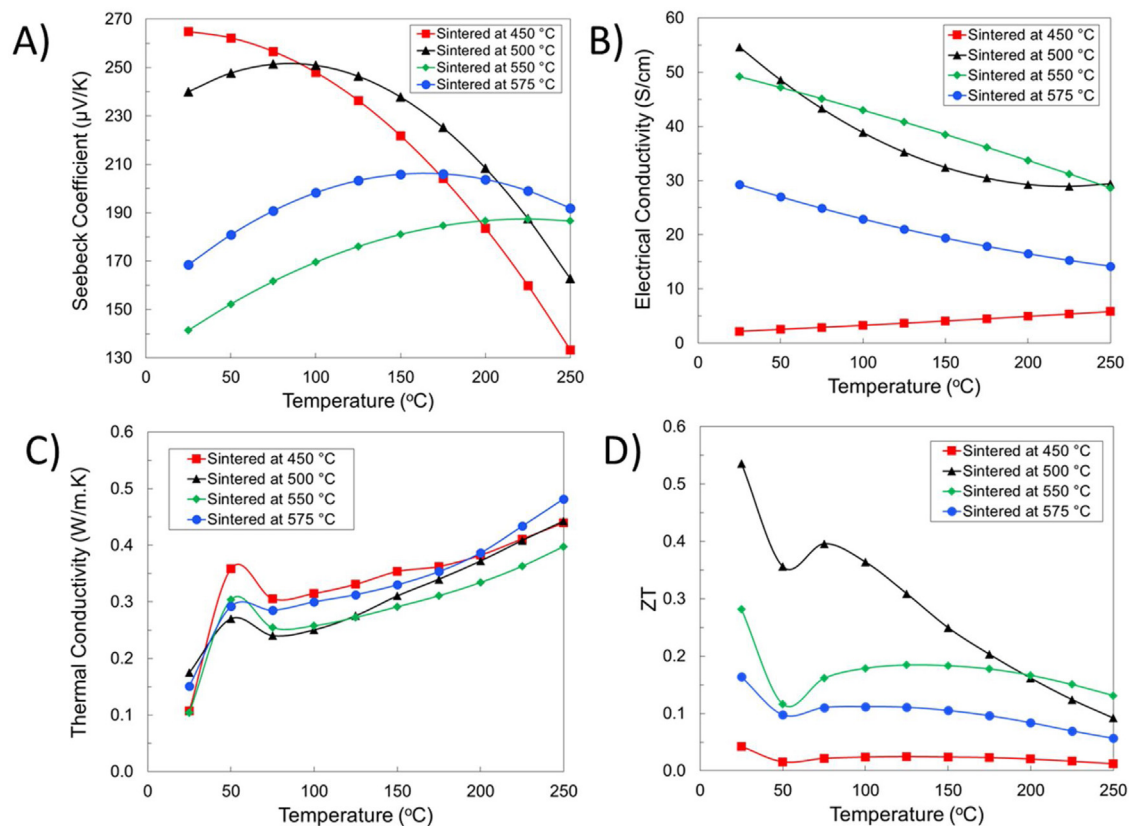
Fig. 4. Temperature dependence of thermoelectric properties of specimens sintered at four different temperatures: (A) Seebeck coefficient, (B) electrical conductivity, (C) thermal conductivity, and (D) dimensionless figure of merit.

conductivity with temperature for all samples might be due to increase in phonon–phonon interaction with temperature. In other words, since the electronic contribution of thermal conductivity in porous samples is quite weak, total thermal conductivity is generally dominated by lattice contribution. Therefore, short wavelength phonon–phonon interaction is enhanced with increasing temperature. SEM pattern and electrical conductivity versus temperature data of our sample also confirm this behavior.

Calculated figure of merit values using these thermoelectric properties according to Eq. (1) are given in Fig. 4D. Specimens sintered at 500 °C showed the highest figure of merit of 0.54 at room temperature. Comparison of figure of merit of FFF printed bismuth telluride samples were found to be significantly higher than those previously reported for SLA printing [23] and dispenser printing [21] which were both reported to be in the range of 0.1–0.2. Up to five fold increase in figure of merit or thermoelectric conversion efficiency of the FFF printed samples showed the versatility of this manufacturing technique. However, printed samples were not as efficient as the bulk bismuth telluride fabricated via conventional methods, the figure of merit of which is around 1.0 at room temperature.

4. Conclusions

Bulk Bi_2Te_3 samples with were additively manufactured using an FFF method while oxidation levels, hierarchical microstructure, and thermoelectric properties were systematically investigated. The results show that the maximum figure of merit for the FFF printed bismuth telluride samples was 0.54, which is nearly five times higher than the thick thermoelectric materials fabricated with SLA and dispenser printing techniques. Enhancement of
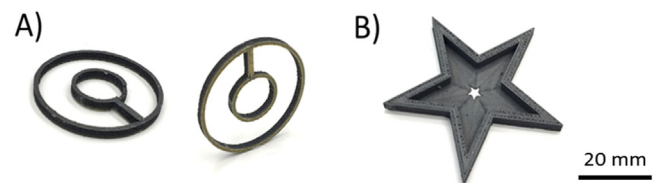
Fig. 5. Pictures of the 3D printed thermoelectric specimens prior to sintering (A) concentric cylinders photographed in two views and (B) 5-point star shaped thermoelectric specimen.

thermoelectric properties, such as Seebeck coefficient and electrical conductivity, is attributed to the lowered porosity of the printed specimens and improved connectivity of the thermoelectric powders sintered at higher temperatures compared to the previous studies. Low contamination and oxidation also played an important role for the enhancement of the material properties. These results evidenced the potential of FFF methods to fabricate thermoelectric materials for practical energy conversion applications regarding the low cost, ease of application, as well as suitable thermoelectric properties. This method rendered fabrication of thermoelectric materials with complex geometry possible, which is otherwise laborious to produce by conventional methods. Fig. 5 shows examples of such complex geometries: concentric cylinders, which could serve as a benchmark for thermoelectric modules or unique heat exchanger applications on circular geometries such as pipes, along with a 5-point star shaped specimen.

Although this study opened a path to further advancements in terms of print quality and the thermoelectric properties compared to the previously reported additive manufacturing methods, overall thermoelectric conversion efficiency still falls behind the bulk

thermoelectric material fabricated via conventional manufacturing methods. The figure of merit (ZT) of bulk Bi_2Te_3 is roughly twice the maximum ZT obtained for additively manufactured samples in this research. This dissimilarity is due to the lowered electrical conductivity of printed samples by high levels of porosity as shown in SEM images. Future efforts will be devoted to mechanical reinforcement strategies to enhance the flexural properties of the filaments for fabrication of larger geometries, enhancement of thermoelectric properties through band engineering, nano-engineering, and doping.

Conflicts of interest

The authors declared no potential conflicts of interest with respect to the research, authorship, and/or publication of this article.

Acknowledgements

Appendix A. Supplementary data

Supplementary data associated with this article can be found, in the online version, at doi:10.1016/j.apmt.2019.01.001.

References

[1] R. Sivaraj, P.K. Rahman, P. Rajiv, H.A. Salam, R. Venckatesh, Biogenic copper oxide nanoparticles synthesis using *Tabernaemontana divaricate* leaf extract and its antibacterial activity against urinary tract pathogen, Spectrochim. Acta A: Mol. Biomol. Spectrosc. 133 (2014) 178–181.
[2] R. Stobart, M. Wijewardane, Z. Yang, Comprehensive analysis of thermoelectric generation systems for automotive applications, Appl. Therm. Eng. 112 (2017) 1433–1444.
[3] M.H. Elsheikh, et al., A review on thermoelectric renewable energy: principle parameters that affect their performance, Renew. Sustain. Energy Rev. 30 (2014) 337–355.
[4] J.P. Heremans, et al., Enhancement of thermoelectric efficiency in PbTe by distortion of the electronic density of states, Science 321 (5888) (2008) 554–557.
[5] A. Ambrosi, k. Sofer, J. Luxa, M. Pumera, Exfoliation of layered topological insulators Bi_2Se_3 and Bi_2Te_3 via electrochemistry, ACS Nano 10 (12) (2016) 11442–11448.
[6] G. Zhou, D. Wang, Few-quintuple Bi_2Te_3 nanofilms as potential thermoelectric materials, Sci. Rep. 5 (2015) 8099.
[7] H. Mamur, M. Bhuiyan, F. Korkmaz, M. Nil, A review on bismuth telluride (Bi_2Te_3) nanostructure for thermoelectric applications, Renew. Sustain. Energy Rev. (2017).
[8] H. Goldsmid, Bismuth telluride and its alloys as materials for thermoelectric generation, Materials 7 (4) (2014) 2577–2592.
[9] M. Orrill, S. LeBlanc, Printed thermoelectric materials and devices: fabrication techniques, advantages, and challenges, J. Appl. Polym. Sci. 134 (3) (2017).
[10] B. Yu, et al., Thermoelectric Property Studies on Thallium-doped Lead Telluride Prepared by Ball Milling Hot Pressing, 2010.
[11] A. Ambrosi, M. Pumera, 3D-printing technologies for electrochemical applications, Chem. Soc. Rev. 45 (10) (2016) 2740–2755.
[12] O. Bubnova, et al., Optimization of the thermoelectric figure of merit in the conducting polymer poly (3,4-ethylenedioxythiophene), Nat. Mater. 10 (6) (2011) 429.
[13] F. Jiao, C.-a. Di, Y. Sun, P. Sheng, W. Xu, D. Zhu, Inkjet-printed flexible organic thin-film thermoelectric devices based on p-and n-type poly (metal 1,1,2,2-ethenetetrathiolate)s/polymer composites through ball-milling, Phil. Trans. R. Soc. A 372 (2013) (2014) 20130008.
[14] T. Juntunen, et al., Inkjet printed large-area flexible few-layer graphene thermoelectrics, Adv. Funct. Mater. 28 (22) (2018) 1800480.
[15] F. Kim, et al., 3D printing of shape-conformable thermoelectric materials using all-inorganic Bi_2Te_3-based inks, Nat. Energy 3 (4) (2018) 301.
[16] Z. Cao, E. Koukharenko, M. Tudor, R. Torah, S. Beeby, Flexible screen printed thermoelectric generator with enhanced processes and materials, Sens. Actuators A: Phys. 238 (2016) 196–206.
[17] R.R. Søndergaard, M. Hösel, N. Espinosa, M. Jørgensen, F.C. Krebs, Practical evaluation of organic polymer thermoelectrics by large-area R2R processing on flexible substrates, Energy Sci. Eng. 1 (2) (2013) 81–88.
[18] T. Varghese, et al., High-performance and flexible thermoelectric films by screen printing solution-processed nanoplate crystals, Sci. Rep. 6 (2016) 33135.
[19] J.H. We, S.J. Kim, G.S. Kim, B.J. Cho, Improvement of thermoelectric properties of screen-printed Bi_2Te_3 thick film by optimization of the annealing process, J. Alloys Compd. 552 (2013) 107–110.
[20] Z. Yuan, et al., Screen-printed radial structure micro radioisotope thermoelectric generator, Appl. Energy 225 (2018) 746–754.
[21] A. Chen, D. Madan, P. Wright, J. Evans, Dispenser-printed planar thick-film thermoelectric energy generators, J. Micromech. Microeng. 21 (10) (2011) 104006.
[22] C. Navone, M. Soulier, M. Plissonnier, A. Seiler, Development of $(Bi,Sb)_2(Te,Se)_3$-based thermoelectric modules by a screen-printing process, J. Electron. Mater. 39 (9) (2010) 1755–1759.
[23] M. He, Y. Zhao, B. Wang, Q. Xi, J. Zhou, Z. Liang, 3D printing fabrication of amorphous thermoelectric materials with ultralow thermal conductivity, Small 11 (44) (2015) 5889–5894.
[24] W.K. Swainson, Method, medium and apparatus for producing three-dimensional figure product, Google Patents, 1977.
[25] J.-P. Kruth, L. Froyen, J. Van Vaerenbergh, P. Mercelis, M. Rombouts, B. Lauwers, Selective laser melting of iron-based powder, J. Mater. Process. Technol. 149 (1-3) (2004) 616–622.
[26] Y. Yan, H. Ke, J. Yang, C. Uher, X. Tang, Fabrication and thermoelectric properties of n-type $CoSb_{2.85}Te_{0.15}$ using selective laser melting, ACS Appl. Mater. Interfaces 10 (16) (2018) 13669–13674.
[27] Y. Mao, et al., Non-equilibrium synthesis and characterization of n-type $Bi_2Te_{2.7}Se_{0.3}$ thermoelectric material prepared by rapid laser melting and solidification, RSC Adv. 7 (35) (2017) 21439–21445.
[28] K. Wu, et al., Preparation of n-type Bi_2Te_3 thermoelectric materials by non-contact dispenser printing combined with selective laser melting, Phys. Stat. Sol.: Rapid Res. Lett. 11 (6) (2017) 1700067.
[29] A. El-Desouky, M. Carter, M.A. Andre, P.M. Bardet, S. LeBlanc, Rapid processing and assembly of semiconductor thermoelectric materials for energy conversion devices, Mater. Lett. 185 (2016) 598–602.
[30] M. Smith, Z. Guan, W. Cantwell, Finite element modelling of the compressive response of lattice structures manufactured using the selective laser melting technique, Int. J. Mech. Sci. 67 (2013) 28–41.
[31] J. Griffey, The types of 3-D printing, Libr. Technol. Rep. 50 (5) (2014) 8–12.
[32] J. Wang, H. Li, R. Liu, L. Li, Y.-H. Lin, C.-W. Nan, Thermoelectric and mechanical properties of PLA/$Bi_{0.5}Sb_{1.5}Te_3$ composite wires used for 3D printing, Compos. Sci. Technol. 157 (2018) 1–9.
[33] C. Satterthwaite, R. Ure Jr., Electrical and thermal properties of Bi_2Te_3, Phys. Rev. 08 (5) (1957) 1164.
[34] E. Rogacheva, I. Krivulkin, O. Nashchekina, A.Y. Sipatov, V. Volobuev, M. Dresselhaus, Effect of oxidation on the thermoelectric properties of PbTe and PbS epitaxial films, Appl. Phys. Lett. 78 (12) (2001) 1661–1663.
[35] E. Rogacheva, et al., Effect of non-stoichiometry on oxidation processes in n-type PbTe thin films, Thin Solid Films 423 (2) (2003) 257–261.
[36] E. Rogacheva, S. Lyubchenko, M. Dresselhaus, Effect of oxidation on thickness dependencies of thermoelectric properties in PbTe/mica thin films, Thin Solid Films 476 (2) (2005) 391–395.
[37] D. Zhao, C. Tian, S. Tang, Y. Liu, L. Chen, High temperature oxidation behavior of cobalt triantimonide thermoelectric material, J. Alloys Compd. 504 (2) (2010) 552–558.